Single Neutral Excitons Confined in AsBr₃ *In Situ* Etched InGaAs Quantum Rings

F. Ding[1, 2, †, *], B. Li[3], N. Akopian[4], U. Perinetti[4], Y. H. Chen[2],
F. M. Peeters[3], A. Rastelli[1], V. Zwiller[4], and O. G. Schmidt[1]

[1] *Institute for Integrative Nanosciences, IFW Dresden, Helmholtzstr 20, D-01069 Dresden, Germany*
[2] *Key Laboratory of Semiconductor Materials Science, Institute of Semiconductors,*
Chinese Academy of Sciences, P.O. Box 912, Beijing 100083, China
[3] *Departement Fysica, Universiteit Antwerpen, Groenenborgerlaan 171, B-2020 Antwerpen, Belgium*
[4] *Kavli Institute of Nanoscience, Delft University of Technology, P.O. Box 5046, 2600 GA Delft, The Netherlands*

We observe the evolution of single self-assembled semiconductor quantum dots into quantum rings during AsBr₃ *in situ* etching. The direct three-dimensional imaging of In(Ga)As nanostructures embedded in GaAs matrix is demonstrated by selective wet chemical etching combined with atomic force microscopy. Single neutral excitons confined in these quantum rings are studied by magneto-photoluminescence. Oscillations in the exciton radiative recombination energy and in the emission intensity are observed under an applied magnetic field. Further, we demonstrate that the period of the oscillations can be tuned by a gate potential that modifies the exciton confinement. The experimental results, combined with calculations, indicate that the exciton Aharonov-Bohm effect may account for the observed effects.

Keywords: Quantum Ring, Quantum Dot, Neutral Exciton, Aharonov Bohm Effect, Gate Controlled, Selective Etching.

1. INTRODUCTION

Self-assembled semiconductor nanostructures, such as quantum dots (QDs) and rings (QRs) are being intensively investigated both because of their possible application in quantum information science, and because they are ideal test beds for fundamental physical research. The Aharonov-Bohm (AB) effect[1] modifies the wave function phase $\Delta\phi$ of a charged particle traveling around a region enclosing a magnetic field. During the 50 years since its discovery, this effect has made a significant impact on the development of physics.[2] The AB effect has been observed independently for electrons and holes in various micro-/nanoscale structures.[3–5]

An interesting question arises here: Is it possible to observe the AB effect when considering a single neutral exciton (an electron–hole pair) confined in a QR? Theoretical investigations have predicted that the phases accumulated by the electron and the hole will be different after one revolution, leading to modulations between different quantum states.[6] And this so called neutral exciton AB effect can be probed from the photoluminescence (PL) emission in semiconductor QRs, since the change in the phase of the exciton wave function is accompanied by a change in the exciton total angular momentum, making the PL emission magnetic field dependent.[6–10] Similar effect has been reported for a *charged exciton* confined in a lithographically defined QR. However, for neutral excitons, the experimental optical observation of this AB-type effect has so far been limited to quantum ring ensembles.[11–13] Considering the relatively small electron–hole separation, the quest for the AB effect in a *single* neutral exciton in a type-I system is quite challenging.

Here we study single self-assembled In(Ga)As/GaAs QRs fabricated by molecular beam epitaxy (MBE) combined with *in situ* AsBr₃ etching.[14] In order to unveil the morphology of buried nanostructures, we use selective chemical etching to remove the GaAs capping layer and investigate the structures with atomic force microscopy (AFM). We observe a progressive morphological evolution of the buried In(Ga)As/GaAs nanostructures, namely, from quantum dots (QDs) to volcano-shaped QRs, as the

---

*Author to whom correspondence should be addressed.
†Present address: IBM Research Zürich, Säumerstrasse 4, 8803 Rüschlikon, Switzerland.

AsBr$_3$ etching depth is increased. Due to a radial asymmetry in the effective confinement for electrons and holes, we expect the neutral exciton AB effect. We observe magnetic field dependent oscillations in the PL energy and intensity of a *single* neutral exciton, in agreement with previous theoretical predictions. We also show that a vertical electric field, which modifies the exciton confinement, is able to control this quantum interference effect.[15]

2. EXPERIMENTAL DETAILS

2.1. Fabrication and Characterization of In(Ga)As/GaAs QRs

All samples examined in this work are grown on semi-insulating GaAs (001) substrates in a solid-source molecular-beam epitaxy system equipped with an AsBr$_3$ gas source. After oxide desorption, a 300-nm GaAs buffer layer is grown at 570 °C. A 1.8-monolayer (ML) InAs layer is then deposited at 500 °C, a temperature which can be easily reproduced by observing the change in surface reconstruction from (2×4) to $c(4 \times 4)$, using an In growth rate of 0.01 ML/s. After 30 s growth interruption, the substrate temperature is lowered to 470 °C and a 10-nm GaAs cap is deposited at a rate of 0.6 ML/s while the temperature is ramped back to 500 °C. After GaAs deposition, the AsBr$_3$ etching gas is subsequently supplied to produce the nanoholes (see the first and second columns of Fig. 1). The etching rate of GaAs was 0.24 ML/s, which was calibrated by reflection high-energy electron diffraction intensity oscillations.

The surface morphology develops into a rhombus-shaped structure with a tiny hole in the middle after 10 nm GaAs overgrowth (see the first row of Fig. 1). After supplying the AsBr$_3$ etching gas, there is a preferential removal of the central part of the *buried* QDs
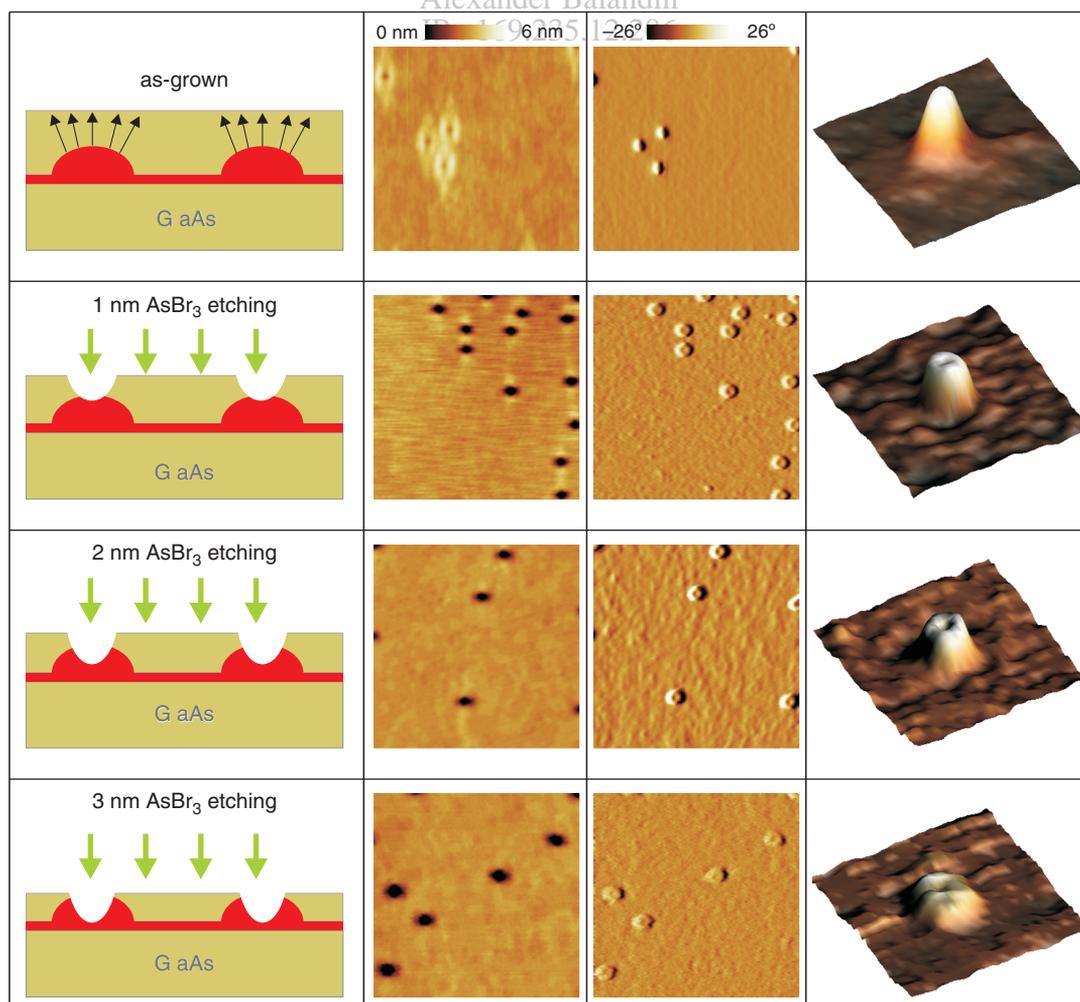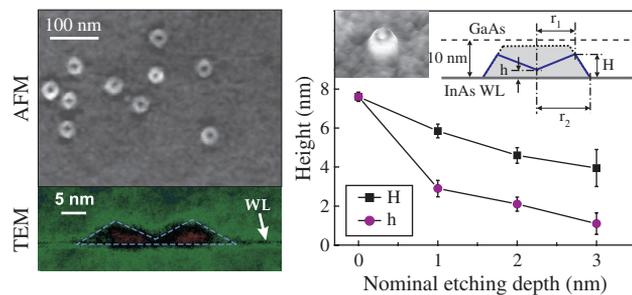
Fig. 1. Fabrication of In(Ga)As/GaAs QRs by MBE combined with AsBr$_3$ *in situ* etching. The first column images show schematic representations of the fabrication processes with different AsBr$_3$ etching depths. 500×500 nm^2 AFM images illustrate the sample surface morphology before (second column) and after (third column) the removal of GaAs capping layer. The last column shows the progressive morphological evolution of a single buried nanostructure, namely, from QD to volcano-shaped QR.

due to the local strain field induced by the buried QDs.[14] In order to characterized the underlying QR structures, a selective chemical etchant [ammonium hydroxide (28% NH₄OH), hydrogen peroxide (31% H₂O₂) and deionized water (1:1:25)] is used to remove the GaAs capping layer. NH₄OH:H₂O₂ solutions are known to etch selectively GaAs over InGaAs alloys.[16–19] The mixture used here etches GaAs at a rate of ~10 nm/s.[17] Figure 1 suggests that the GaAs cap is completely removed by the solution and the etching process significantly slows down at the In(Ga)As wetting layer (WL) (see also Fig. 2). Prolonged etching ($\gtrsim$ 2–3 seconds) results in the removal of the WL and the undercut of the QDs. We verified that different etching experiments with the same nominal duration (1 second) performed on the same sample yield compatible results. Slower etching rates of GaAs are achievable with diluted solutions.[20]

We observe from Figure 1 that, by varying the nominal AsBr₃ etching depth, the morphology of the QR structure can be tuned (see the second, third and fourth rows). The statistical structural analysis of the uncapped In(Ga)As nanostructures as a function of the nominal etching depth is given in the right part of Figure 2. A cross sectional transmission electron microscopy (TEM) image of a single QR from a similar sample is also presented (Fig. 2), further supporting the validity of our method. We argue that the selective chemical etching combined with AFM is a reliable, fast and convenient way to characterize buried In(Ga)As/GaAs nanostructures, it provides information on the three-dimensional morphology and does not require any special sample preparation.

We focus now on the QRs with a nominal etching depth of 3 nm. Both AFM and TEM (see Fig. 2) confirm that the average inner radius r_1 of the QR is about 8.5 nm, while the average outer radius r_2 is about 19 nm, and the height H is about 4 nm. The inner height h is less than 1 nm. Such a ring structure could produce different confinement
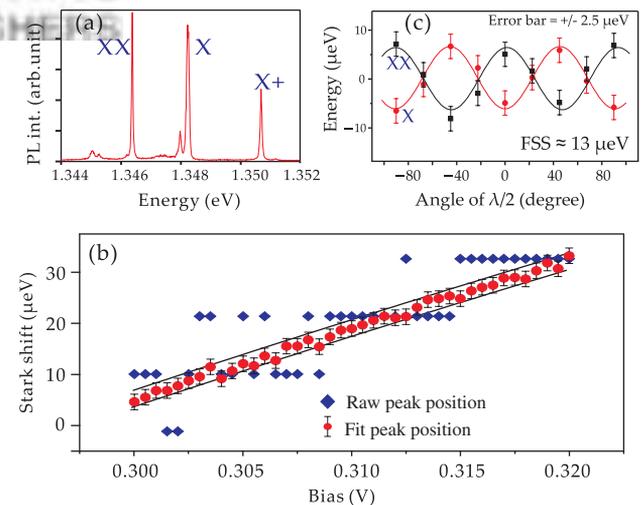
potentials for the electron and the hole, thus the neutral exciton AB can be expected.

2.2. Magneto-Photoluminescence

We use magneto-PL to probe the energy changes and intensity changes related to the nature of the ground state. The samples are placed in a cryostat tube which is evacuated and then refilled with a small amount of helium exchange gas. The tube is then inserted into a 4.2 K helium bath dewar equipped with a superconducting magnet capable of providing fields up to 9 T. The sample is excited by a 532 nm laser beam and the PL is collected by an objective with 0.85 numerical aperture. The PL signal is dispersed by a spectrometer with 0.75 m focal length equipped with a 1800 g/mm grating, and captured by a liquid nitrogen cooled Si charge-coupled device (CCD). Figure 3(a) shows a typical PL spectrum for a single QR at $B = 0$ T. We use power-dependent PL, polarization-dependent PL (Fig. 3(c)), and charging experiments[21] to identify the neutral exciton X, the biexciton XX, and charged exciton X⁺.

We have carefully optimized and tested the system to minimize drifts associated with magnetic field ramping. An optimum resolution of 2.5 μeV can be achieved by fitting the PL peaks with Lorentzian functions. The accuracy of this peak-determination procedure is determined by using the quantum confined Stark effect (QCSE). Some of the QRs are embedded in an n-i-Schottky structure, consisting of 20 nm n^+ GaAs layer followed by a 20 nm thick spacer layer under the QRs, 30 nm i-GaAs and a 116 nm thick AlAs/GaAs short period superlattice. With a 5 nm thick semi-transparent Ti top gate, an electric field can be applied to modify the energy band of the ring.[21, 22] When

Fig. 2. AFM image shows the QRs with nominal AsBr₃ etching depth of 3 nm after removal of the GaAs capping layer by selective chemical etching. The lower graph shows the cross sectional TEM image of a single QR from the similar sample. The statistical structural analysis of the uncapped In(Ga)As nanostructures as a function of the nominal etching depth is given in the right part. H is the height of the embedded nanostructures, and h is the distance between the InAs WL and the bottom of the dip at the nanostructure apex.

Fig. 3. (a) Typical PL spectrum for a single QR. (b) The PL peak is shifted by QCSE, both fit peak positions and the measured raw peak positions are plotted. (c) Linear polarization dependent energy shift of X and XX. The solid lines are sine wave fittings.

a forward bias V_g is scanned from 0.3 to 0.32 V (with steps of 0.5 mV), the PL emission energy of a single QR is tuned by about 30 μeV (see Fig. 3(b)). We observe that, in contrast to the discretized raw data (diamond points), the Lorentzian fit data show a smooth blue-shift of the peak positions (round points). We plot the 95% prediction band of the fit function in Figure 3(b) (solid lines), from which an error of ±1.5 μeV for this Lorentzian analysis procedure is estimated. For the evaluation of the systematic error, repeated measurements (B field increasing and decreasing) are performed on the same QR and the fit peak positions are reproducible to within ±2.5 μeV. We can therefore expect an overall error of ±2.5 μeV in the peak-determination procedure used in this work.

To further support the validity of this peak determination procedure, we perform the FSS measurements for X and XX lines (Fig. 3(c)). The data points are given by Lorentzian fits, with an uncertainty of 2.5 μeV. Solid lines in the exciton and biexciton plots are sine wave fitting curves. As expected, X and XX show anti-correlated shifts as we rotate the half-wave plate. The FSS of this QD is only 13 μeV, which is near the resolution limit of our PL system and would be undetectable without the Lorentzian fitting process.

A magnetic field up to 9 T is applied along the sample growth direction, and we observe the characteristic Zeeman splitting as well as the diamagnetic shift of the PL emission energy (see Fig. 4(a)), similar to previous reports on single QRs.[23] In Figure 4(b) we plot the *neutral* exciton emission energies of the QR after averaging the emission energy values of the Zeeman split lines. It is observed

that the emission energy does not scale quadratically with increasing B field. From its shape, Figure 4(b) looks quite similar to the one shown in a very recent report,[13] in which AB oscillations in *ensemble* InAs/GaAs QRs were observed. However, the diamagnetic shift for a single QR studied in our work is ~6 times smaller than the value for the *ensemble* QRs in Ref. [13]. and the oscillation amplitude is much smaller. Also, no Zeeman splitting was observed in Ref. [13] because of the broad ensemble emission. In order to visualize the magnetic field induced oscillations, we subtract a single parabola from Figure 4(b) and plot the results in Figure 4(c). We observe two maxima at ~4 T and ~7 T (the solid line here, which represents the smoothed data using a Savitzky-Golay filter, is guide to the eye), suggesting changes in the ground state transitions.

Another significant feature observed is the decrease in PL intensity with increasing magnetic field, see Figure 4(d). The change in PL intensity is one of the signatures expected for a QR and is attributed to oscillations in the ground state transitions.[6, 11–13] Two knees can be observed at ~4 T and ~7 T (Fig. 4(c)), which correspond well with the peak energy oscillation maxima in Figure 4(c) (indicated by arrows).

All the observations here are well above the system resolution, and they strongly contrast with the experimental results on a conventional QD, where no peak energy oscillation and PL intensity quenching were observed, see Ref. [15]. Especially, the PL intensity of this QR quenches by more than 70% with increasing magnetic field, which is confirmed by repeating the measurements and similar observations in other QRs. A recent study on single GaAs
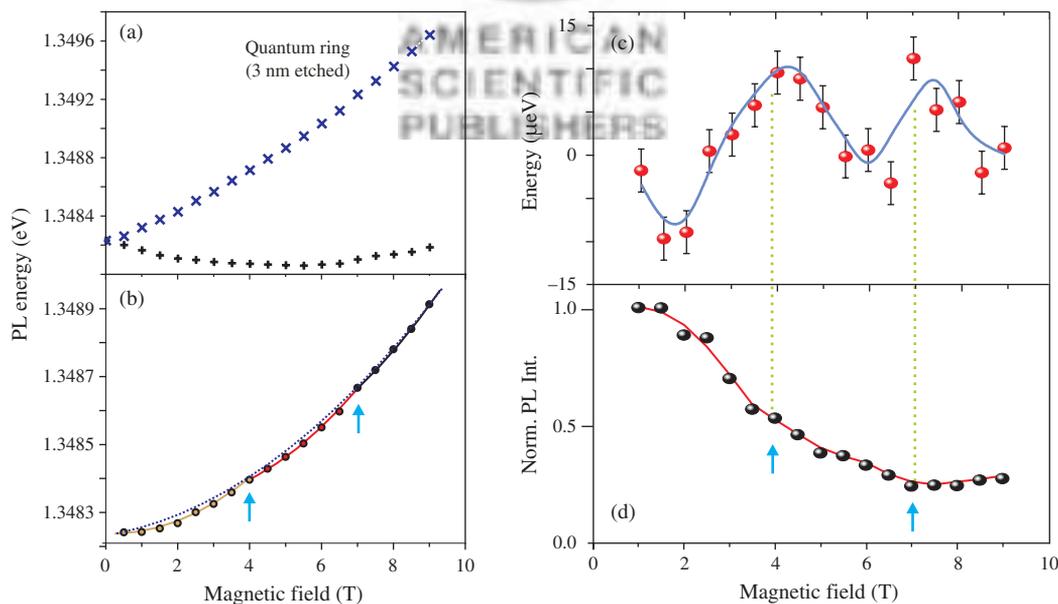

Fig. 4. Fitted PL peak position versus B field before (a) and after (c) averaging the Zeeman splitting for the neutral exciton emission in a 3 nm-etched QR. The blue dashed line in (b) indicates a parabolic fit. Oscillations in PL energy and corresponding normalized PL intensity as a function of B field are shown in (c) and (d), respectively. The solid lines represent the smoothed data using a Savitzky-Golay filter. The arrows in (b) and (d) indicate changes in the ground state transitions.

QR obtained by droplet epitaxy also revealed a significant reduction in the PL intensity by more than 20% at $B > 6$ T,[24] the exciton AB effect may account for the observation.

2.3. Gate-Controlled Oscillations

We use the above mentioned gated-QR structure to demonstrate the possibility of controlling the observed effect with an external electric field. The oscillations for a single QR (with a nominal AsBr₃ etching depth of 3 nm) under a forward bias of 2.8 V are clearly seen in Figure 5(a), with the two transition points at 2.6 T and 8 T. The PL intensity also shows similar quenching behavior as in Figure 4(d) (not shown here). When we decrease the bias from 2.8 V to 0.8 V, it is clear that the transition points shift smoothly to higher magnetic fields (Fig. 5(b)), indicating that the effective radii of the electron and the hole are modified by the external gate potential. The PL intensity is also strongly modified at different electric fields, which is a consequence of the QCSE. At ~1.8 V the PL intensity reaches an overall maximum and then decreases, see Ref. [15]. Interestingly, the PL intensity at 1.8 V shows clear modulation by the magnetic field, i.e., first quenches by more than 25%
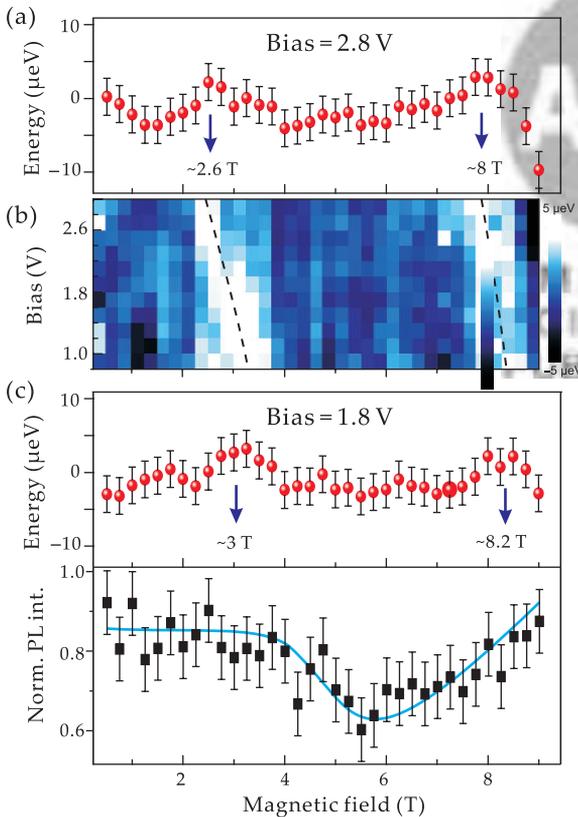
and then recovers fully to its original value with increasing magnetic field (Fig. 5(c)). This observation is quite similar to the long-existed theoretical prediction for a weakly bound neutral exciton confined in a QR.[6]

3. DISCUSSIONS

Previous theoretical works distinguish between excitons composed of strongly and weakly bound electron–hole pairs.[6] In Ref. [7], the effectiveness of the electron–hole Coulomb interaction is expressed as:
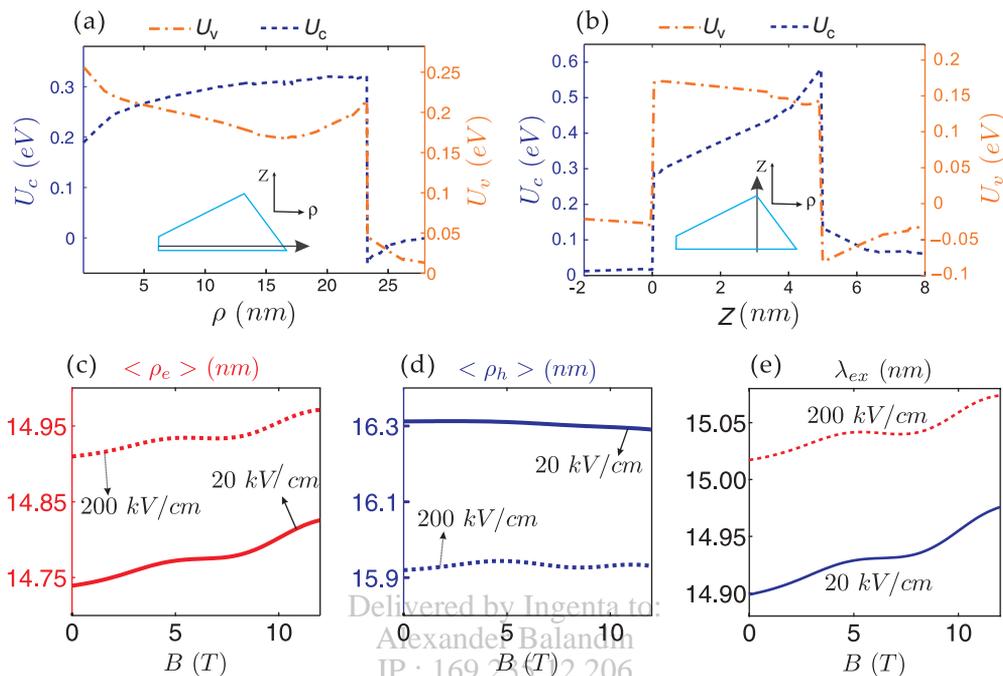
$$v_q = \frac{e^2}{\pi \epsilon_r \sqrt{R_e R_h}} Q_{|q|-1/2}\left(1 + \frac{|R_e - R_h|}{2R_e R_h}\right) \quad (1)$$

where ϵ_r is the dielectric constant, and $Q_\mu(x)$ is the Legendre function. In the strongly bound regime where v_q is dominant, the exciton moves along the ring as one tightly bound particle and AB effect manifests itself in a bright to dark transition in the ground state with increasing magnetic field. While in the opposite limit of a weakly bound electron–hole pair, an interesting modulation between different bright and dark states should appear. The electron–hole pairs in above-mentioned QRs are close to the weakly bound regime, this is because:

(i) in the ring geometry the ratio of Coulomb to kinetic energies is proportional to the ring radius, while for small rings ($R < a^*$, the effective Bohr radius) the quantization due to kinetic motion is strong[6, 25] and the effectiveness of v_q becomes weaker;

(ii) in our structure the n-doped layer which locates 20 nm under the QRs (also, the metal contact in the gated structure) can sufficiently screen the effectiveness of v_q;[7]

(iii) in experiment we also observe that the changes in the binding energies $\Delta E_B(XX) \approx \Delta E_B(X^+)$ when E changes (not shown here), indicating that the strongly confined few-particle picture is valid in our QRs and, the effective radii of electron and hole are very different.[26, 27]

However, the theory in Ref. [6] is not sufficient to explain our results. We model a simplified QR as depicted in Figure 2 with the main aim to explain the gate-controlled oscillation effect (Fig. 5). The ground state energy of the neutral exciton inside the In₁₋ₓGaₓAs ring (surrounded by GaAs barrier) is calculated within the configuration interaction (CI) method. For simplicity, the presence of a wetting layer, azimuthal anisotropy[28] and structural asymmetry[23] are not included in calculation. More details of the calculation can be found in Ref. [15].

The indium composition inside the ring and the large lattice mismatch between the ring and barrier materials result in a considerably large strain, and this strain has a different effect on the electron and hole confinement potential. With finite element methods we can calculate the strain induced shift to the band offset, U_c and U_v. Note that we take the opposite value of the hole confinement potential so that the larger value of U_v stands for higher energy.

Fig. 5. (a) Under a forward bias of 2.8 V the PL energy shows clear transitions at ~2.6 T and ~8 T. (b) When the bias changes from 2.8 V to 0.8 V, the transitions shift smoothly to higher magnetic fields. (c) At 1.8 V the PL energy shows transitions at ~3 T and ~8.2 T, while the normalized PL intensity also shows oscillations.

Fig. 6. (a) Strain induced shift to the band offset, U_c and U_v along horizontal direction ρ and, (b) along vertical direction Z. The inset shows half cross-section of the QR structure. The effective radius of the electron (c) and the hole (d) is calculated at two different electric fields. (e) The radius $\lambda_{ex} = ((m_h + m_e)/(m_h/ < \rho_e >^2 + m_e/ < \rho_h >^2))^{0.5}$, shows similar behavior to $\langle \rho_e \rangle$.

We plot U_c and U_v along different directions ρ and Z in Figures 6(a and b). It is clear that the strain induced band offset for the electron is smaller in the area with smaller ρ and Z, while for the hole the top area of the QR has the lowest value. So the presence of strain makes the electron and the hole apart from each other, which is important for the observation of the neutral exciton AB effect.

We now examine the effects of electric field and magnetic field on the effective radius of the electron (hole) $\langle \rho_e \rangle$ ($\langle \rho_h \rangle$). From Figure 6(c) we know that with decreasing vertical electric field from 200 kV/cm to 20 kV/cm, the electron is attracted to the bottom area of the ring, decreasing its effective radius, while the hole is pushed to the top of the ring and its effective radius increases (Fig. 6(d)). However, from the change of $\langle \rho_e \rangle$ and $\langle \rho_h \rangle$ alone we can not conclude that the period of the AB oscillation decreases. Theoretical study reveals that the oscillation comes from a change in the value of the angular momentum pair (l_e, l_h), not from the single electron or hole angular momentum. The period of the oscillation is not only related to the effective radius of the electron and the hole, but also to their effective masses.

In our calculation it is found that the magnetic field at which the first transition takes place is proportional to $\hbar/e\lambda_{ex}^2$, where $1/\lambda_{ex}^2 = (m_h/\langle \rho_e \rangle^2 + m_e/\langle \rho_e \rangle^2)/(m_e + m_h)$. We plot λ_{ex} as a function of magnetic field for different values of electric field in Figure 6(e). Because the effective mass of the hole is much larger than that of the electron (also because the electron and the hole radii change within the same magnitude), λ_{ex} should have a

similar behavior as the electron effective radius $\langle \rho_e \rangle$. This is clearly observed in Figure 6(e) and λ_{ex} decreases monotonically with decreasing electric field. As a result, the first transition takes place at a higher magnetic field when we decrease the electric field (see Fig. 5(b)). The explanation for the second transition is similar, although the formula for the magnetic field at which it takes place is different (it also has the dominant term $m_h/\langle \rho_e \rangle^2$), which shifts to higher magnetic field when the electric field decreases.

Previous reports revealed that the PL intensity also oscillates with magnetic field and the oscillation amplitudes are around 5%~10%.[12, 13] This should explain the intensity oscillation in Figure 5(c). However, for the QRs studied in Figures 4 and 5 (at 2.8 V), we observe strong quenching in the PL intensity. This phenomenon originates partly from the AB-like quantum interference effect, but there is also contribution from the imperfect ring geometry. Grochol et al. demonstrated that even a *slightly* eccentric ring geometry can smooth the oscillations and renders the total angular momentum a non-well defined quantum number.[10] The selection rules are only strictly applicable in a system with perfect rotational symmetry, and at high magnetic fields an oscillator strength transfer is expected between excitonic bright states and dark states.

4. CONCLUSION

In conclusion, we fabricate a novel self-assembled In(Ga)As/GaAs QR structure by MBE combined with *in situ* AsBr$_3$ etching. The morphology of In(Ga)As

nanostructures embedded in GaAs matrix is unveiled by selective wet chemical etching combined with AFM, and we find that the structural parameters of the QRs can be well controlled by the AsBr$_3$ etching depth. Single *neutral* excitons confined in the volcano-like QRs are studied by magneto-photoluminescence. Oscillations in both PL energy and intensity are observed under an applied magnetic field. We also show that the oscillations can be tuned by applying a vertical electric field which modifies the electron and hole effective radii. Although the experimental features are not fully understood yet, a theoretical investigation is able to explain the main results. We conclude that the exciton Aharonov-Bohm effect may account for the observed effects.

References and Notes

1. Y. Aharonov and D. Bohm, *Phys. Rev.* 115, 485 (**1959**).
2. S. Popescu, *Nat. Phys.* 6, 151 (**2010**).
3. A. G. Aronov and Y. Sharvin, *Rev. Mod. Phys.* 59, 755 (**1987**).
4. S. Zaric, G. N. Ostojic, J. Kono, J. Shaver, V. C. Moore, M. S. Strano, R. H. Hauge, R. E. Smalley, and X. Wei, *Science* 304, 1129 (**2004**).
5. A. Fuhrer, S. Luscher, T. Ihn, T. Heinzel, K. Ensslin, W. Wegscheider, and M. Bichler, *Nature* 413, 822 (**2001**).
6. A. O. Govorov, S. E. Ulloa, K. Karrai, and R. J. Warburton, *Phys. Rev. B* 66, 081309 (**2002**).
7. Luis G. G. V. Dias da Silva, S. E. Ulloa, and T. V. Shahbazyan, *Phys. Rev. B* 72, 125327 (**2005**).
8. R. A. Römer and M. E. Raikh, *Phys. Rev. B* 62, 7045 (**2000**).
9. A. Chaplik, *JETP Lett.* 62, 900 (**1995**).
10. M. Grochol, F. Grosse, and R. Zimmermann, *Phys. Rev. B* 74, 115416 (**2006**).
11. E. Ribeiro, A. O. Govorov, W. Carvalho, and G. Medeiros-Ribeiro, *Phys. Rev. Lett.* 92, 126402 (**2004**).
12. I. R. Sellers, V. R. Whiteside, I. L. Kuskovsky, A. O. Govorov, and B. D. Mccombe, *Phys. Rev. Lett.* 100, 136405 (**2008**).
13. M. D. Teodoro, V. L. Campo, Jr., V. Lopez-Richard, E. Marega, Jr., G. E. Marques, Y. Galvão Gobato, F. Iikawa, M. J. S. P. Brasil, Z. Y. AbuWaar, V. G. Dorogan, Yu. I. Mazur, M. Benamara, and G. J. Salamo, *Phys. Rev. Lett.* 104, 086401 (**2010**).
14. F. Ding, L. Wang, S. Kiravittaya, E. Müller, A. Rastelli, and O. G. Schmidt, *Appl. Phys. Lett.* 90, 173104 (**2007**).
15. F. Ding, N. Akopian, B. Li, U. Perinetti, A. Govorov, F. M. Peeters, C. C. Bof Bufon, C. Deneke, Y. H. Chen, A. Rastelli, O. G. Schmidt, and V. Zwiller, *Phys. Rev. B* 82, 075309 (**2010**).
16. D. G. Hill, K. L. Lear, and J. S. Harris, Jr., *J. Electrochem. Soc.* 137, 2912 (**1990**).
17. S.-J. Paik, J. Kim, S. Park, S. Kim, C. Koo, S.-K. Lee, and D. D. Cho, 42, 326 (**2003**).
18. Z. M. Wang, L. Zhang, K. Holmes, and G. J. Salamo, *Appl. Phys. Lett.* 86, 143106 (**2005**).
19. B. N. Zvonkov, I. A. Karpovich, N. V. Baidus, D. O. Filatov, S. V. Morozov, and Y. Y. Gushina, *Nanotechnology* 11, 221 (**2000**).
20. L. Wang, A. Rastelli, S. Kiravittaya, P. Atkinson, F. Ding, C. C. Bof Bufon, C. Hermannstädter, M. Witzany, G. J. Beirne, P. Michler, and O. G. Schmidt, *New J. Phys.* 10, 045010 (**2008**).
21. R. J. Warburton, C. Schaflein, D. Haft, F. Bickel, A. Lorke, K. Karrai, J. M. Garcia, W. Schoenfeld, and P. M. Petroff, *Nature* 405, 926 (**2000**).
22. B. D. Gerardot, S. Seidl, P. A. Dalgarno, R. J. Warburton, D. Granados, J. M. Garcia, K. Kowalik, O. Krebs, K. Karrai, A. Badolato, and P. M. Petroff, *Appl. Phys. Lett.* 90, 041101 (**2007**).
23. T.-C. Lin, C.-H. Lin, H.-S. Ling, Y.-J. Fu, W.-H. Chang, S.-D. Lin, and C.-P. Lee, *Phys. Rev. B* 80, 081304 (**2009**).
24. T. Kuroda, T. Belhadj, T. Mano, B. Urbaszek, T. Amand, X. Marie, S. Sanguinetti, K. Sakoda, and N. Koguchi, *Phys. Stat. Sol. (b)* 246, 861 (**2009**).
25. M. Korkusiński, P. Hawrylak, and M. Bayer, *Phys. Stat. Sol. (b)* 234, 273 (**2002**).
26. F. Ding, R. Singh, J. D. Plumhof, T. Zander, V. Křápek, Y. H. Chen, M. Benyoucef, V. Zwiller, K. Dörr, G. Bester, A. Rastelli, and O. G. Schmidt, *Phys. Rev. Lett.* 104, 067405 (**2010**).
27. M.-F. Tsai, H. Lin, C.-H. Lin, S.-D. Lin, S.-Y. Wang, M.-C. Lo, S.-J. Cheng, M.-C. Lee, and W.-H. Chang, *Phys. Rev. Lett.* 101, 267402 (**2008**).
28. V. M. Fomin, V. N. Gladilin, J. T. Devreese, N. A. J. M. Kleemans, M. Bozkurt, and P. M. Koenraad, *Phys. Stat. Sol. (b)* 245, 2657 (**2008**).
29. M. Bayer, M. Korkusinski, P. Hawrylak, T. Gutbrod, M. Michel, and A. Forchel, *Phys. Rev. Lett.* 90, 186801 (**2003**).
30. R. J. Warburton, C. Schulhauser, D. Haft, C. Schäflein, K. Karrai, J. M. Garcia, W. Schoenfeld, and P. M. Petroff, *Phys. Rev. B* 65, 113303 (**2002**).